泥页岩中有机质：类型、热演化与有机孔隙

期刊：	《地球科学》
稿件 ID	ES-2022-0043.R2
稿件类型：	综述
作者提交的日期：	2022-3-17
完整作者列表：	刘, 贝; 中国地质大学（武汉），资源学院
关键词：	泥页岩, 分散有机质, 显微组分, 热演化, 固体沥青, 有机孔隙
研究方向：	页岩油气, 有机岩石学, 非常规油气

1
2
3
4
5
6
7
8
9
10
11
12
13
14
15
16
17
18
19
20
21
22
23
24
25
26
27
28
29
30
31
32
33
34
35
36
37
38
39
40
41
42
43
44
45
46
47
48
49
50
51
52
53
54
55
56
57
58
59
60

泥页岩中有机质：类型、热演化与有机孔隙

刘贝

中国地质大学（武汉）构造与油气资源教育部重点实验室，湖北武汉 430074

中国地质大学（武汉）资源学院，湖北武汉 430074

摘要: 泥页岩中的有机质作为石油和天然气的来源，其有机岩石学分类方案仍不明确，传统的煤岩学分类方法并不完全适用于泥页岩中的分散有机质。页岩中有机孔隙是页岩孔隙系统的重要组成部分，在很大程度上控制了页岩的含气量和孔隙度，但其成因及与有机质类型和热成熟度的关系仍存在争议。本文系统地总结了泥页岩中分散有机质的类型、不同类型有机质的热演化特征以及有机孔隙发育与保存的控制机理，并指出了存在问题及今后研究方向。泥页岩中的分散有机质包含 5 个显微组分组：镜质体、惰质体、类脂体、动物碎屑和次生有机质，每个显微组分组可再划分为多个显微组分。不同显微组分的成因和生烃潜力不同，有机孔隙发育程度也存在差异。页岩中有机孔隙包括原生孔隙和次生孔隙，后者是主要的有机孔隙类型，其形成与生油型有机质生烃密切相关，主要赋存在固体沥青或焦沥青中。有机质类型和成熟度决定了次生有机孔隙的发育程度，而热成熟度、有机质含量、矿物组成和孔隙压力控制了其保存程度。烃源岩评价中对有机质生烃潜力的研究应建立在对显微组分以及不同显微组分生烃能力充分了解的基础上。非常规油气储层表征中对有机孔隙的研究应充分考虑有机质数量、类型、成熟度以及页岩矿物学组成，准确地评价有机孔隙对页岩孔隙系统的贡献。

关键词: 泥页岩；分散有机质；显微组分；热演化；固体沥青；有机孔隙

中图分类号: P588

Organic matter in shales: Types, thermal evolution, and organic pores

Bei Liu

Key Laboratory of Tectonics and Petroleum Resources of Ministry of Education, China University of Geosciences, Wuhan, 430074

School of Earth Resources, China University of Geosciences, Wuhan, 430074

Abstract: Organic matter (OM) in mudstone/shales is the source of oil and gas, the organic petrographic classification of which has not reached a consensus. Traditional coal petrological methods do not completely apply to dispersed organic matter (DOM) in shales. OM-hosted pores are important constituents of the pore system in shale reservoirs, and they, to a large degree, control the gas content and porosity of shales. However, the origin of organic pores and their relationships with OM type and thermal maturity remain controversial. This study systematically summarized the types of DOM in shales, thermal evolution of different types of OM,

作者简介：刘贝（1989–），男，教授，主要从事非常规油气地质研究. ORCID: 0000-0003-1146-1227. E-mail: liubei12@cug.edu.cn

30 and factors controlling the formation and preservation of organic pores, and proposed the issues related to

31 DOM study and future research directions. DOM in shales can classified into five maceral groups: vitrinite,

32 inertinite, liptinite, zooclasts, and secondary organic matter, with each group consisting of multiple macerals.

33 Different macerals have different origins, and varying potential of hydrocarbon generation and development of

34 organic pores. Organic pores in shales can be primary or secondary, the latter of which is the dominant type.

35 Secondary organic pores occur in solid bitumen or pyrobitumen, and their development is related to thermal

36 maturation of oil-prone macerals. The development of secondary organic pores is controlled by OM type and

37 thermal maturity, and their preservation depends on thermal maturity, OM content, mineralogical composition

38 of shales, and pore pressure. When conducting source rock evaluation, the hydrocarbon generation potential of

39 OM should be studied based on a good understanding of maceral types, composition, and their hydrocarbon

40 generation potential. In order to accurately assess the contribution of organic pores to the pore system of shale

41 reservoirs, the influence of OM type, content, and thermal maturity should be taken into consideration.

42 **Key words:** dispersed organic matter; shale; maceral; thermal evolution; solid bitumen; organic pores

43 **0 引言**

44 　　泥页岩中有机质是石油和天然气的物质来源，其丰度、类型和成熟度是常规和非常规石油系统的

45 关键参数（Tissot and Welte, 1984; Peters and Cassa, 1994; Passey et al., 2010; Jarvie, 2012a, 2012b;

46 Hackley and Cardott, 2016; Mastalerz et al., 2018; Liu et al., 2022）。根据 H/C 和 O/C 原子比或岩石热解

47 （Rock-Eval）的氢指数（HI）和氧指数（OI），可以将泥页岩中有机质划分为四种干酪根类型（Peters

48 and Cassa, 1994），而有机岩石学方法根据有机质的反射率、形态、结构以及荧光性，可将泥页岩中有

49 机质划分为多种显微组分（Potter et al., 1998; Stasiuk et al., 2002; Hackley and Cardott, 2016; Flores and

50 Suárez-Ruiz, 2017; Mastalerz et al., 2018; Liu et al., 2022）。根据元素分析划分的干酪根类型与根据岩石

51 学特征划分的显微组分可建立对应关系：I 型干酪根主要以藻类体或无定形体为主，生烃能力最高；II

52 型干酪根生烃能力中等，主要以无定形体为主；III 型干酪根生烃能力较差，主要以生气为主，对应显

53 微组分为镜质体；IV 型干酪根基本无生烃能力，主要以惰质体为主（Peters and Cassa, 1994; Liu et al.,

54 2019, 2022）。因此，分析泥页岩中有机质的类型以及不同类型有机质的生烃潜力和热演化特征对常规

55 烃源岩评价和非常规油气储层表征具有重要的意义。

56 　　页岩中有机孔隙是页岩储层孔隙系统的重要组成部分（Loucks et al., 2009, 2012; Schieber, 2010;

57 Mastalerz et al., 2013; Katz and Arango, 2018; 腾格尔等, 2021; Liu et al., 2022），控制着页岩的含气量、

58 甲烷吸附能力和孔隙度（Ross and Bustin, 2009; Hao et al., 2013; 陈国辉等, 2020; 邱振等, 2020; Liu et al.,

59 2021）。有机孔隙的孔径一般小于 1000 nm（Loucks et al., 2012），位于有机质大分子结构中的孔隙小于

60 1 nm（Bousige et al., 2016）。有机孔隙一般认为是在有机质生烃和排烃过程中产生的（Loucks et al.,

61 2012; Liu et al., 2017, 2022）。不同类型有机质的生烃潜力不同，有机孔隙的发育程度也不同。有机孔

62 隙的描述一般是利用扫描电镜对 Ar 离子抛光的页岩表面进行观察（Loucks et al., 2009, 2012; Schieber,

63 2010, 2013），但扫描电镜下无法有效地区分有机质类型（Liu et al., 2017, 2022），造成有机孔隙赋存状

64 态及成因机制仍存在争议。

65 　　我国页岩油气资源丰富（赵文智等, 2020; 邹才能等, 2020; 邹才能和邱振, 2021），页岩中有机质生

66 烃能力和有机孔隙发育程度是页岩油气勘探开发过程中的重要研究内容，目前对页岩中分散有机质类

67 型以及热演化模式仍缺乏深入的研究。本文的目的是系统地总结泥页岩中有机质的类型、不同类型有

68 机质在热成熟过程中的演化特征以及有机孔发育与保存的控制机理。本文有望提高对泥页岩中分散有

69 机质以及有机孔隙的认识，并对常规烃源岩评价和非常规油气储层表征提供指导。

70 **1 泥页岩中有机质类型**

71 　　泥页岩中分散有机质类型的划分源自煤岩学，国内外不同学者建立了不同的分类方案

72 （Teichmüller, 1986; 肖贤明和金奎励, 1990; 王飞宇等, 1993; 刘大锰等, 1995; 涂建琪等, 1998, 2012），

73 然而目前并没有统一的分类体系。当前国际上常用的分类方案将泥页岩中有机质划分为 5 个显微组分

74 组：镜质体、惰质体、类脂体、动物碎屑和次生有机质，每个显微组分组包含多种显微组分（Potter

75 et al., 1998; Stasiuk et al., 2002; Hackley and Cardott, 2016; Flores and Suárez-Ruiz, 2017; Mastalerz et al.,

76 2018; Liu et al., 2022）。其中，镜质体、惰质体和类脂体的划分与煤岩学显微组分的划分基本一致

77 （ICCP, 1998, 2001; Pickel et al., 2017; 代世峰等, 2021a, 2021b, 2021c），唯一的区别在于渗出沥青体

78 （次生有机质）的归类。由于泥页岩中含有大量的生油型类脂体，这些组分在生烃之后生成大量的沥

79 青，因此将次生有机质单独列为一个显微组分组。次生有机质包括固体沥青、焦沥青和油。动物碎屑

80 主要包括笔石、几丁虫等动物碎屑。本文以国际分类方案为准（表 1）。

81

82　表 1 页岩中显微组分分类方法（修改自 Stasiuk et al., 2002; Mastalerz et al., 2018; Liu et al., 2022）

83　**Table 1 Classification of macerals in shales (Modified from Stasiuk et al., 2002; Mastalerz et al., 2018;**

84　**Liu et al., 2022)**

| 显微组分组	显微组分	备注	扫描电镜下特征
镜质体 **Vitrinite** (III 型干酪根)	镜质结构体 Telinite 胶质结构体 Collotelinite 镜质碎屑体 Vitrodetrinite 胶质碎屑体 Collodetrinite 团块凝胶体 Corpogelinite 凝胶体 Gelinite	由于页岩中镜质体含量较少，并且粒径较小，识别不同的显微组分非常困难。因此，不适合划分显微组分。对于镜质体含量较高的页岩，仍可根据ICCP System 1994镜质体分类方案划分出不同的显微组分。	以分散颗粒状存在于页岩基质中。
惰质体 **Inertinite** (IV 型干酪根)	丝质体 Fusinite 半丝质体 Semifusinite 真菌体 Funginite 粗粒体 Macrinite 分泌体 Secretinite 微粒体 Micrinite 惰质碎屑体 Inertodetrinite	同镜质体一样，页岩中惰质体含量较少且粒径较小，因此不适合划分显微组分。对于惰质体含量较高的页岩，仍可根据ICCP System 1994惰质体分类方案划分出不同的显微组分。丝质体、半丝质体和惰质碎屑体是页岩中常见的惰质体。	以分散颗粒状存在于页岩基质中。部分惰质体具有细胞结构，可以作为鉴定标志。如果细胞结构不存在，很难与镜质体区分。
类脂体 **Liptinite** (I 型或 II 型干酪根)	藻类体 Alginite 无定形体 Amorphinite (Bituminite/amorphous organic matter) 类脂碎屑体 Liptodetrinite 孢子体 Sporinite 角质体 Cutinite 木栓质体 Suberinite 树脂体 Resinite 叶绿素体 Chlorophyllinite	藻类体、无定形体（又称沥青质体）和类脂碎屑体是页岩中常见的生油型组分，其它来自高等植物的显微组分在页岩中不常见，特别是海相页岩。	藻类体由于其特有的形态在扫描电镜下较易识别。垂直层理面时为棒状，平行层理面时为圆形。生油型藻类体一般不存在于生油高峰（R_o 0.8–1.0%）之后。 无定形体无固定形态，以条带状或透镜状存在于页岩基质中，通常含有粘土级的矿物包裹体。生油型无定形体一般不存在于生油高峰（R_o 0.8–1.0%）之后。
动物碎屑 **Zooclasts**	笔石 Graptolite 几丁虫 Chitinozoa 虫颚 Scolecodonts 有孔虫 Foram liners	在部分页岩中存在。其反射率可以用于成熟度评价，特别是在前泥盆系页岩中。	以分散颗粒状存在于页岩基质中。动物碎屑可以根据其形貌特征鉴定。如果动物碎屑粒径较小且无识别特征，不易与镜质体和惰质体区分。

次生有机质 Secondary organic matter	固体沥青 Solid bitumen	生油高峰（R_o 0.8–1.0%）之后，富含I和II型干酪根页岩中主要的有机质类型。	固体沥青和焦沥青的赋存状态相似，以充填的形式存在于颗粒间孔或颗粒内部。低成熟度时，固体沥青和无定形体较难区分。
	焦沥青 Pyrobitumen	干气窗内，富含 I 和 II 型干酪根页岩中主要的有机质类型。焦沥青和固体沥青的成熟度临界值为固体沥青反射率1.5%。对于含硫有机质，临界值为1.3%。	
	油 Oil	只存在于生油窗内。	以油滴形式存在。

85

1.1 镜质体（Vitrinite）

87 　煤和泥页岩中的镜质体来自陆源高等植物，由植物的木质纤维组织经凝胶化而形成（韩德馨,
88 1996; Taylor et al., 1998）。镜质体反射率（R_o）介于惰质体和类脂体反射率之间，是最常用的热成熟度
89 指标（Mukhopadhyay and Dow, 1994）。泥页岩中的镜质体随陆源碎屑搬运而来，因此其通常以分散颗
90 粒形式存在于页岩基质中（图 1）。由于其粒径较小，一般不具备细胞结构。油浸反射光下，镜质体呈
91 深灰色至亮白色，颜色随成熟度增加而变浅。页岩中镜质体一般不显荧光。相对湖相页岩，海相页岩
92 中镜质体含量较少。Mastalerz et al. (2018) 建议由于页岩中镜质体含量较少，且粒径较小，镜下鉴别不
93 同的显微组分非常困难，因此不适合划分显微组分。但对于镜质体含量较高的页岩，如煤系地层中的
94 页岩，仍可根据 ICCP System 1994 镜质体分类方案（ICCP, 1998; 代世峰等, 2021a）划分出不同的显微
95 组分。
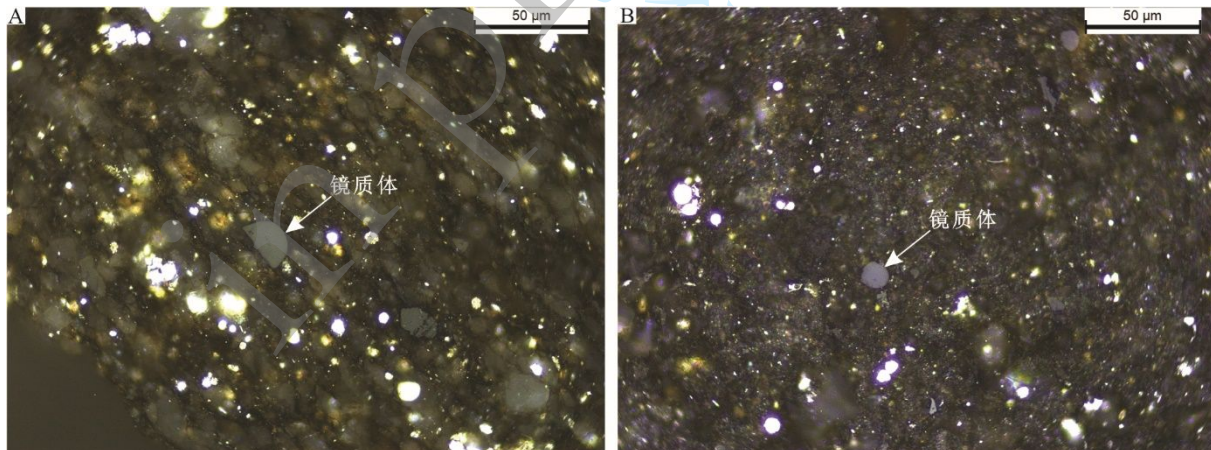
96
97 图 1 页岩中镜质体显微照片，油浸反射光。美国 Illinois 盆地 New Albany 页岩，R_o 0.55%
98 Fig. 1 Photomicrographs of vitrinite in reflected white light and oil immersion. New Albany Shale of the Illinois Basin, R_o 0.55%
99

1.2 惰质体（Inertinite）

101 　同镜质体一样，煤和泥页岩中的惰质体来自陆源高等植物，不同的是惰质体在沉积之前通常经历
102 火焚或氧化（韩德馨, 1996; Taylor et al., 1998）。煤岩学三个显微组分组（镜质体、惰质体和类脂体）
103 中，惰质体的芳香化程度和反射率最高，基本无生烃能力。同镜质体一样，惰质体也是以分散颗粒形

104 式存在于页岩基质中，但惰质体通常具有来自植物胞腔的细胞结构（图2），可据此在扫描电镜下区分

105 镜质体和惰质体。油浸反射光下，惰质体呈亮白色，其颜色变化随成熟度增加不明显。惰质体在荧光

106 下不显荧光。丝质体、半丝质体和惰质碎屑体是页岩中常见的惰质体。如果页岩中惰质体含量较少，

107 通常没有必要再划分显微组分。如果页岩中惰质体含量较高，可根据 ICCP System 1994 惰质体分类方

108 案（ICCP, 2001; 代世峰等, 2021b）划分不同的显微组分。

109
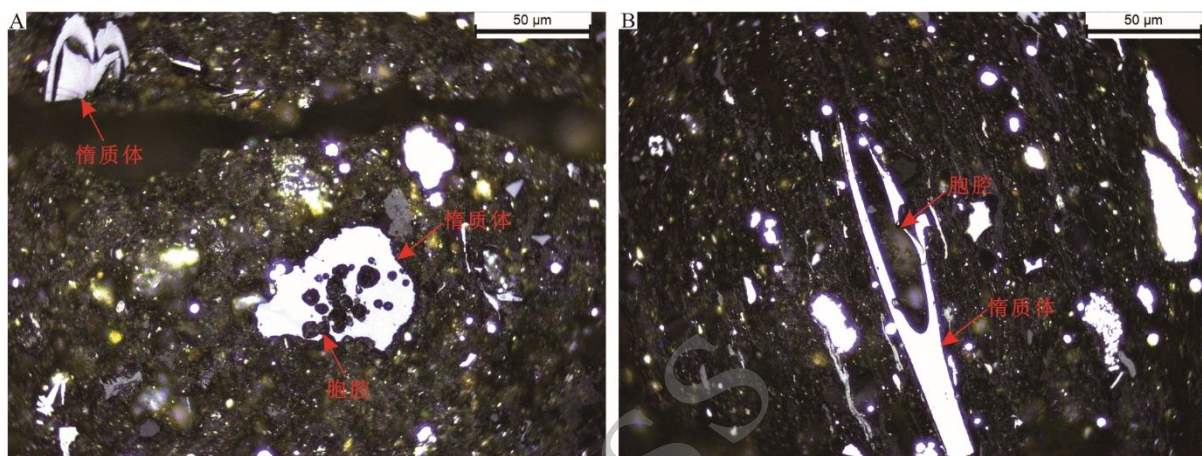
110 图 2 页岩中惰质体显微照片，油浸反射光。美国 Illinois 盆地 New Albany 页岩，R_o 0.55%

111 Fig. 2 Photomicrographs of inertinite in reflected white light and oil immersion. New Albany Shale of the Illinois Basin, R_o

112 0.55%

113

1.3 类脂体（Liptinite）

115 　　类脂体是泥页岩中含量最高的显微组分组，也是泥页岩生烃的主要贡献者。富含类脂体的泥页岩

116 中有机质的类型通常为 I 型或 II 型干酪根。煤岩学三个显微组分组（镜质体、惰质体和类脂体）中，

117 类脂体的反射率最低（Pickel et al., 2017; 代世峰等, 2021c）。泥页岩中的类脂主要包括藻类体、无定形

118 体（又称沥青质体）和类脂碎屑体（表 1），其它来自高等植物的显微组分，如孢子体、角质体、树脂

119 体在泥页岩中不常见，尤其是海相页岩。有些研究将腐泥组（sapropelinite）单独划分为一个显微组分

120 组（王飞宇等, 1993），其对应的显微组分主要为无定形体和藻类体。

121 　　藻类体来自浮游藻类，具有极高的生烃潜力。*Botryococcus, Tasmanites* 和 *Leiosphaeridia* 是泥页岩

122 中最常见的藻类。源自 *Tasmanites* 孢囊的藻类体普遍存在于北美上泥盆统页岩中，如 Illinois 盆地的

123 New Albany 页岩，Michigan Basin 的 Antrim 页岩，Appalachian Basin 盆地的 Ohio 页岩和盆地南部的

124 Chattanooga 页岩，Williston 盆地的 Bakken 页岩，其氢指数高达 900 mg 烃 / g 总有机碳（TOC）

125 （Vigran et al., 2008）。未成熟或低成熟时，藻类体在油浸反射光下呈琥珀色，在蓝光下显黄绿色荧光

126 （图 3）。随着成熟度的增加，藻类体颜色逐渐加深，荧光由黄绿色逐渐变为黄色、橙色和褐色，荧光

127 强度逐渐降低，最终在 R_o 0.9%时转变为前油沥青，荧光消失（肖贤明和金奎励, 1991; Hackley et al.,

128 2017; Liu et al., 2019）。根据藻结构的保存程度，藻类体可划分为结构藻类体（telalginite）和层状藻类

129　体（lamalginite）（Kus et al., 2017; Pickel et al., 2017; 代世峰等, 2021c）。结构藻类体指的是结构保存完

130　整的藻（图 3），而层状藻类体呈条带状分布，平行于层理面，通常是细菌降解的产物。如果层状藻类

131　体遭受更强程度的细菌降解，其结构更难以识别，荧光性减弱甚至消失，逐渐转变为无定形体（Teng

132　et al., 2021）。

133　　　无定形体（又称沥青质体）指的是显微镜下观察到的没有固定结构的显微组分（图 4; Kus et al.,

134　2017; Teng et al., 2021），在泥页岩中普遍存在。因为成熟泥页岩中含有大量的固体沥青（次生有机质），

135　而沥青质体（bitiminite）与沥青（bitumen）容易混淆，因此通常用无定形体（amorphinite）或无定形

136　有机质（amorphous organic matter）来命名页岩中原生无定形有机质。无定形通常含有粘土级的矿物包

137　裹体（Liu et al., 2020a），因此也被称为矿物沥青基质（mineral-bituminous groundmass）。无定形体来自

138　被细菌降解的浮游植物、浮游动物和细菌（Kus et al., 2017; Teng et al., 2021）。根据荧光性、反射率、

139　和结构，可以将无定形体进一步划分为多种类型（Thompson and Dembicki, 1986; Senftle et al., 1987;

140　Kus et al., 2017; Teng et al., 2021）。Thompson and Dembicki (1986) 根据显微结构的差异将无定形体划分

141　为四种类型。Senftle et al. (1987) 根据荧光性将无定形体划分为荧光无定形体（fluoramorphinite）和非

142　荧光无定形体（hebamorphinite）。Teng et al. (2021) 根据反射率高低将无定形体划分为低反射率无定形

143　体（low-reflectance amorphous organic matter）和微粒化无定形体（micrinized amorphous organic matter）。

144　　　类脂碎屑体以类脂体碎片的形式存在于页岩基质中，其颜色和荧光性与藻类体相似（图 4），可能

145　来自破碎的藻类体碎片。
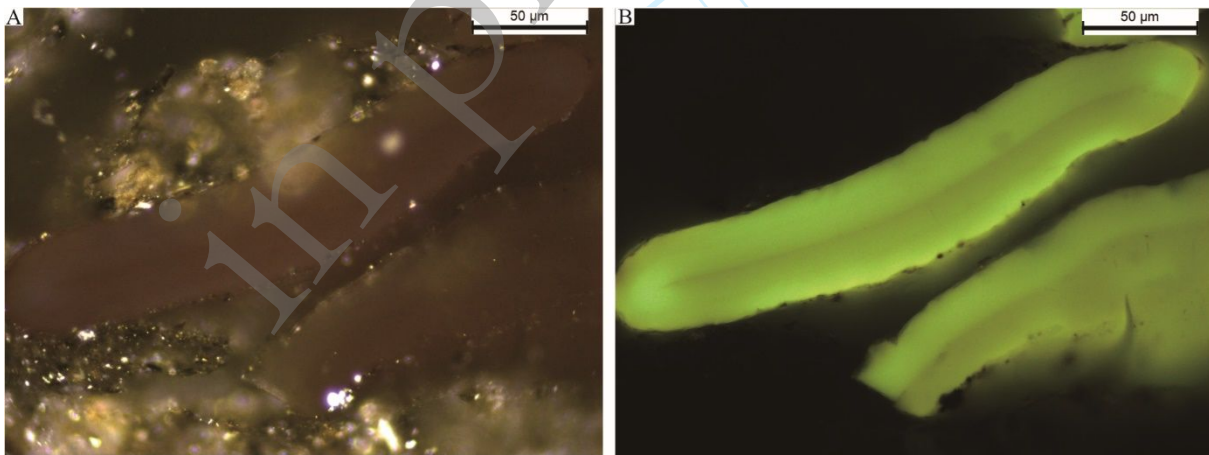
146

147　图 3 页岩中藻类体显微照片，油浸反射光（A）和荧光（B）。美国 Illinois 盆地 New Albany 页岩，R_o 0.55%

148　Fig. 3 Photomicrographs of alginite in reflected white light and oil immersion (A) and in fluorescence mode (B). New Albany

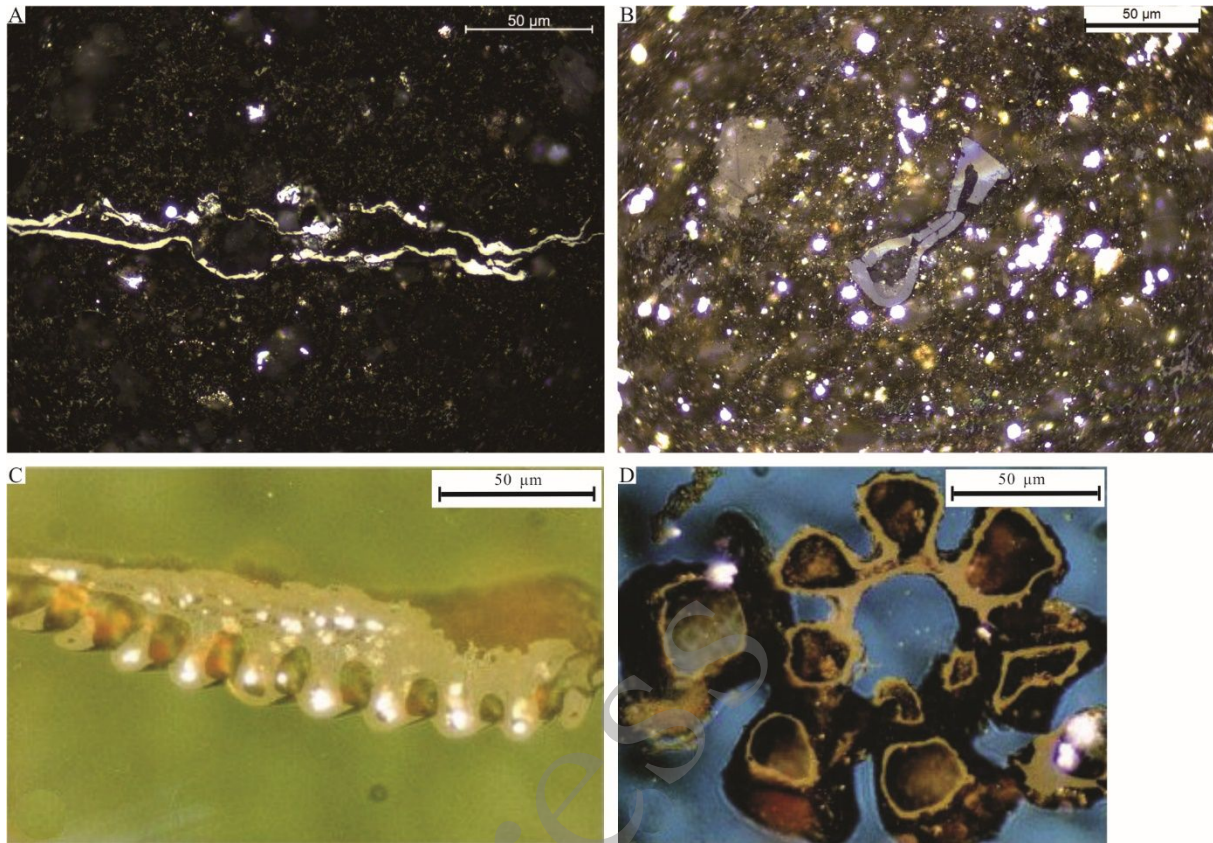149　Shale of the Illinois Basin, R_o 0.55%

150
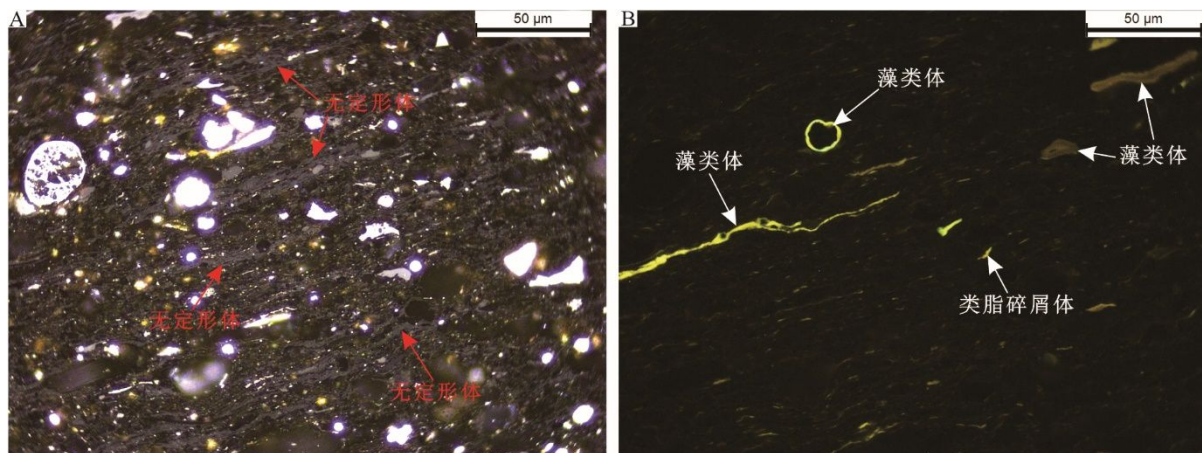
图 4 页岩中无定形体显微照片，油浸反射光（A）和荧光（B）。美国 Illinois 盆地 New Albany 页岩，R_o 0.55%

Fig. 4 Photomicrographs of amorphinite in reflected white light and oil immersion (A) and in fluorescence mode (B). New Albany Shale of the Illinois Basin, R_o 0.55%

1.4 动物碎屑（Zooclasts）

动物碎屑来自浮游动物的碎片。泥页岩中可以识别的浮游动物主要包括笔石、几丁虫、虫颚、有孔虫（表 1）。动物碎屑的生烃潜力较低，与镜质体相似，但相对镜质体较低。在不含镜质体的泥页岩中，尤其是前泥盆系泥页岩中，动物碎屑的反射率可以代替镜质体反射率作为成熟度指标（Bertrand and Héroux, 1987; Goodarzi and Norford, 1989; Bertrand, 1990; Petersen et al., 2013），例如我国四川盆地上奥陶统-下志留统五峰组-龙马溪组页岩（Luo et al., 2017, 2020; 王晔等, 2019）。

油浸反射光下，动物碎屑呈深灰色至亮白色，成熟度越高，颜色越浅。高成熟度时，笔石发育各向异性，双折射率增加（Luo et al., 2020）。荧光下，笔石在低成熟度时显暗褐色荧光，高成熟度时荧光消失。在显微镜和扫描电镜下观察时，动物碎屑可根据其形貌特征来区分，例如几丁虫的墨水瓶结构（图 5）。当动物碎屑粒径较小且无识别特征时，很难与镜质体区分（Petersen et al., 2013; Liu et al., 2020b），在前泥盆系地层中通常被认定为类镜质体或镜状体（vitrinite-like particles）（Buchardt and Lewan, 1990）。

图 5 页岩中动物碎屑显微照片，油浸反射光。（A）笔石，四川盆地五峰组-龙马溪组页岩，等效镜质体反射率 EqR$_o$ 3.07%。（B）几丁虫，美国 Illinois 盆地 New Albany 页岩，R$_o$ 0.79%（Liu et al., 2022）。（C）虫颚，加拿大西北地区 Ramparts 组。（D）有孔虫，瑞士侏罗纪地层。C 和 D 来自 Potter et al. (1998)

Fig. 5 Photomicrographs of zooclasts in reflected white light and oil immersion. (A) Graptolite. Wufeng-Longmaxi Shale of the Sichuan Basin. Equivalent vitrinite reflectance EqR$_o$ 3.07%. (B) Chitinozoa. New Albany Shale of the Illinois Basin, R$_o$ 0.79% (Liu et al., 2022). (C) Scolecodont. Ramparts Formation, Northwest Territories, Canada. (D) Foramnifera liners. Jurassic, Switzerland. C 和 D from Potter et al. (1998)

1.5 次生有机质（Secondary organic matter）

次生有机质是生油型有机质在热演化过程中转化而来的，包括固体沥青、焦沥青和油（表 1）。生油高峰（R$_o$ 0.8–1.0%）之后，固体沥青成为泥页岩中主要的有机质类型（Hackley and Cardott, 2016; Mastalerz et al., 2018; Liu et al., 2019, 2022; Sanei, 2020）。此处的固体沥青是有机岩石学定义的，不同于有机地球化学定义的沥青，即可以用有机溶剂（如氯仿）抽提的可溶有机质（Durand, 1980）。

固体沥青包括前油沥青（pre-oil bitumen）和后油沥青（post-oil bitumen）（Mastalerz et al., 2018）。前油沥青指的是生油之前的沥青，由生油型有机质转化而来，而后油沥青指的是生油之后的沥青，也就是常见的固体沥青（Mastalerz et al., 2018; Liu et al., 2019, 2022）。因为有机质生油是一个连续的过程，在生油窗内某一成熟度，前油沥青、后油沥青和正在生油过程中的沥青可能同时存在（Liu et al., 2019,

186　2022），区分不同的沥青较为困难，可以统称为固体沥青。显微镜下固体沥青和焦沥青的形态结构与赋

187　存状态相似，但在化学结构、溶解性和生烃潜力方面差异巨大：焦沥青芳香化程度更高、不溶解于有

188　机溶剂、基本无生烃能力 (Mastalerz et al., 2018)。Mastalerz et al. (2018) 综合考虑光学特征、化学结构、

189　溶解性和成因，建议固体沥青和焦沥青的成熟度临界值为固体沥青反射率 1.5%，而对于含硫有机质，

190　该临界值为 1.3%。Mastalerz et al. (2018) 和 Sanei (2020) 系统总结了页岩中固体沥青的成因、演化以及

191　物理和化学性质。

192　　　固体沥青的反射率和镜质体反射率一般呈正相关关系，因此可用来表征不含镜质体泥页岩的成熟

193　度（丰国秀和陈盛吉, 1988; Jacob, 1989; Landis and Castaño, 1995; Schoenherr et al., 2007; Hackley and

194　Cardott, 2016; 仰云峰, 2016; Mastalerz et al., 2018; Liu et al., 2019; Schmidt et al., 2019; 徐学敏等, 2019; 王

195　晔等, 2020）。然而，页岩中沥青存在多种类型，并不是每种沥青的反射率均可用来表征热成熟度。根

196　据结构特征和反射率值，可将页岩中焦沥青划分为微粒化沥青、均质沥青和各向异性沥青 (Mastalerz et

197　al., 2018)。均质沥青表面平整干净，反射率分布集中，可以用来表征页岩成熟度（Landis and Castaño,

198　1995)；微粒化沥青由细小颗粒组成，表面粗糙，反射率通常低于均质沥青；各向异性沥青呈现焦炭结

199　构，双折射率高，其形成可能与原油组分或压力有关 (Stasiuk, 1997; Mastalerz et al., 2018)。微粒化沥青

200　和各向异性沥青均不适合用来表征页岩成熟度。

201　　　油浸反射光下，固体沥青呈黑色（前油沥青）、深灰色至灰色，成熟度越高，颜色越浅；焦沥青一

202　般呈浅灰色至亮白色（图 6）。荧光下，除前油沥青和部分反射率较低的固体沥青显红褐色荧光外，固

203　体沥青和焦沥青一般不显荧光。固体沥青主要赋存在颗粒间或颗粒内部，因为其在生油窗内曾是高粘

204　度流体，通常呈现充填特征（Liu et al., 2019, 2022)，可据此在扫描电镜下与其它组分区分。
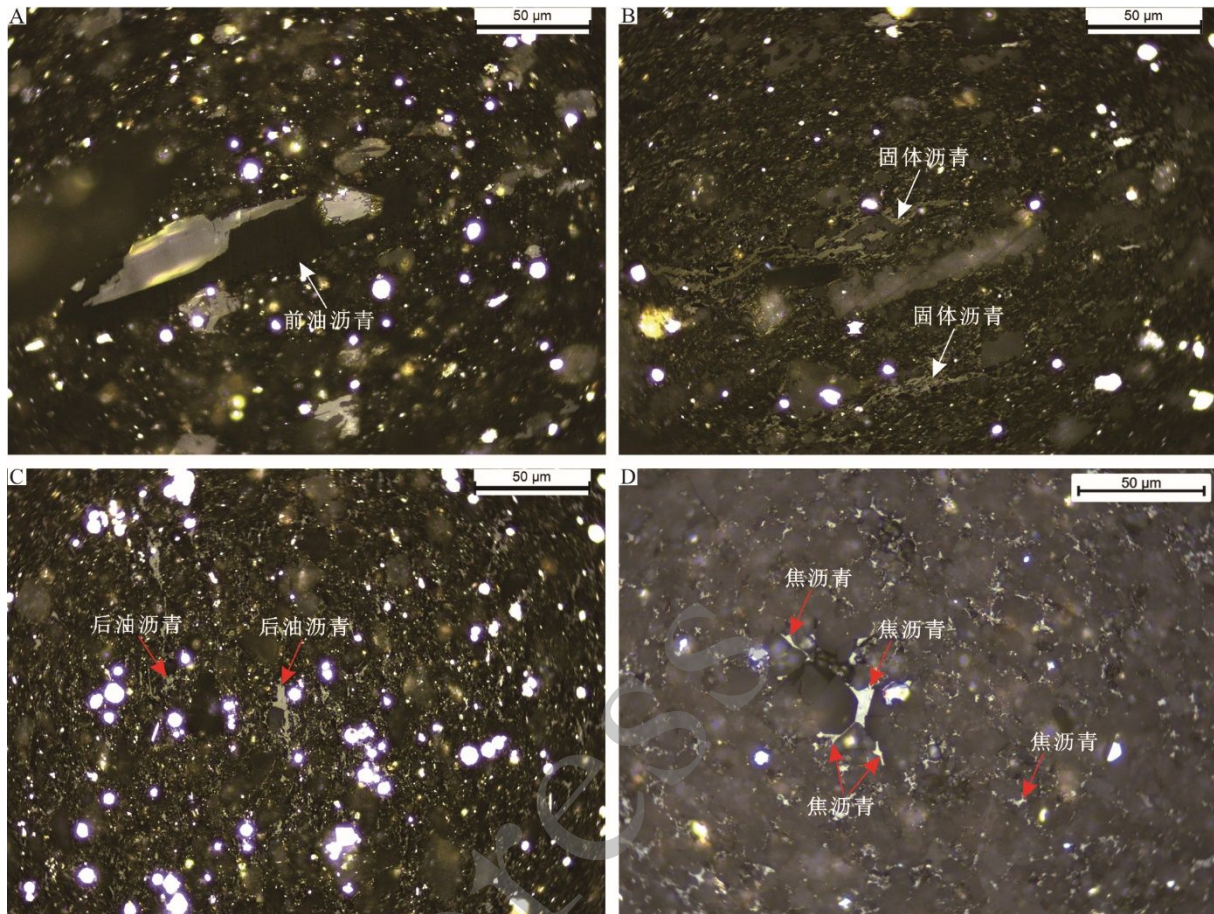
图 6 页岩中固体沥青和焦沥青显微照片，油浸反射光。（A）来自藻类体的前油沥青。藻类体的形状仍可识别出，表明大量生烃仍未开始。美国 Illinois 盆地 New Albany 页岩，R_o 0.84%。（B）生油高峰阶段的固体沥青。美国 Illinois 盆地 New Albany 页岩，R_o 0.98%。（C）凝析油和湿气阶段的后油沥青。美国 Illinois 盆地 New Albany 页岩，R_o 1.18%。（D）干气窗内的焦沥青。美国 Appalachian 盆地 Marcellus 页岩，R_o 2.41%

Fig. 6 Photomicrographs of solid bitumen and pyrobitumen in reflected white light and oil immersion. (A) Pre-oil bitumen transformed from alginate. Alginite can still be identified based on morphology, suggesting that significant hydrocarbon generation has not started yet. New Albany Shale of the Illinois Basin, R_o 0.84%. (A) Solid bitumen in the peak oil window. New Albany Shale of the Illinois Basin, R_o 0.98%. (C) Solid bitumen in the condensate-wet gas window. New Albany Shale of the Illinois Basin, R_o 1.18%. (D) Pyrobitumen in the dry gas window. Marcellus Shale of the Appalachian Basin, R_o 2.41%

2 有机质热演化

不同显微组分的成因不同，生烃潜力也存在差异（肖贤明和金奎励, 1991）。类脂体生烃能力最高，镜质体和动物碎屑次之，惰质体基本无生烃能力（肖贤明和金奎励, 1991）。热演化过程中，镜质体、惰质体和动物碎屑的形貌特征未表现出明显变化，在过成熟泥页岩中仍可识别出这三种显微组分组（Liu et al., 2022），而类脂体在热演化过程中形貌特征变化较为显著（Liu et al., 2022）。以藻类体为例，藻类体在生油窗内首先通过沥青化过程转化为前油沥青，随着成熟度的增加，前油沥青逐渐转化为油

222 气和后油沥青，后油沥青在干气窗内转化为焦沥青，同时油也会在干气窗内二次裂解为焦沥青（图 7;

223 Liu et al., 2022）。因此，如果未成熟或低成熟页岩中有机质以生油型类脂体为主，生油高峰（R_o 0.8–

224 1.0%）之后，页岩中的有机质则以固体沥青或焦沥青为主（Hackley and Cardott, 2016; Mastalerz et al.,

225 2018; Liu et al., 2019, 2022），生油型藻类体在高成熟度页岩中基本不存在。例如，美国 Appalachian 盆

226 地的上泥盆统 Ohio 页岩和 Illinois 盆地的上泥盆统 New Albany 页岩中，成熟度达到 R_o 1.0%之后，来

227 自 *Tasmanites* 孢囊的藻类体全部消失，转化为油气和固体沥青（Ryder et al., 2013; Liu et al., 2019）。高

228 成熟度页岩中，例如我国四川盆地的上奥陶统-下志留统五峰组-龙马溪组页岩和美国 Appalachian 盆地

229 的中泥盆统 Marcellus 页岩，有机质主要以焦沥青为主。值得注意的是，五峰组-龙马溪组页岩中笔石

230 普遍存在（Luo et al., 2016; 王晔等, 2019），在某些特定层段，有机质可能以笔石为主。我国南方海相

231 页岩成熟度普遍较高，等效镜质体反射率高达 4.0%以上。在过成熟阶段，随着成熟度增加，焦沥青芳

232 香性增强，反射率增加，各向异性增强，逐渐向石墨转化，导致其孔隙度和电阻率降低，影响页岩的

233 测井评价（王玉满等, 2014）。在过高成熟阶段（$R_o > 4.0\%$），随着成熟度增加，有机质比表面积出

234 现降低的趋势（王保忠等，2019），这可能是由于有机质芳香性增强，分子结构堆积得更加致密，导致

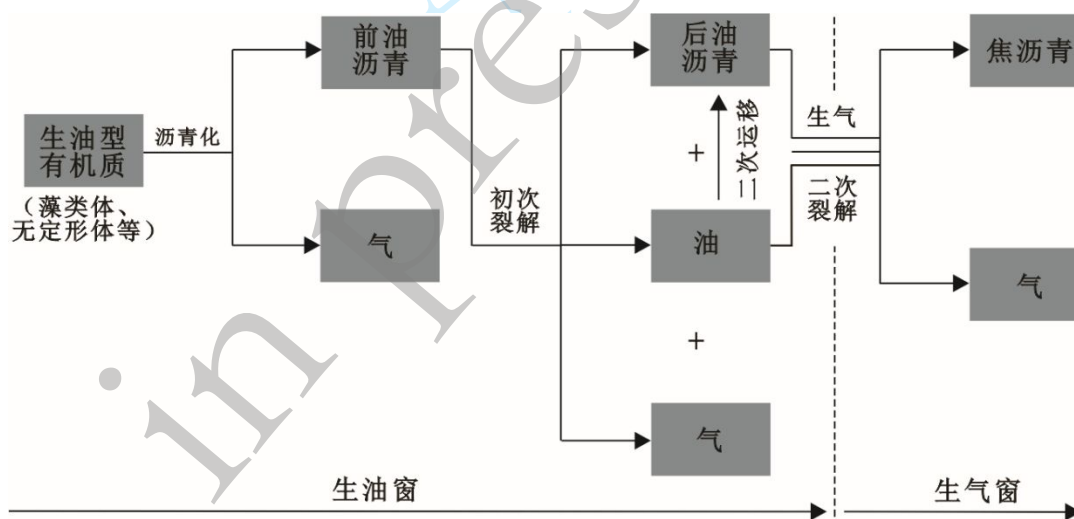235 微孔减少（Liu et al., 2022）。

236

237 图 7 热演化过程中生油型有机质的演化路径（来自 Liu et al., 2022; 参考自 Jarvie et al., 2007; Bernard and Horsfield, 2014;

238 Camp, 2016; Mastalerz et al., 2018）

239 Fig. 7 Evolutionary pathway of oil-prone organic matter during thermal maturation (From Liu et al., 2022; Modified from Jarvie

240 et al., 2007; Bernard and Horsfield, 2014; Camp, 2016; Mastalerz et al., 2018)

241

3 有机孔隙发育与保存

243 　　页岩中的有机孔隙（图 8）是页岩储层孔隙系统的重要组成部分（Loucks et al., 2009, 2012;

244 Schieber, 2010; Curtis et al., 2012; Milliken et al., 2013; 腾格尔等, 2021）。自从 Loucks et al. (2009) 首次报

245　导美国 Fort Worth 盆地 Barnett Shale 页岩中有机孔隙以来，有机孔隙的成因、发育、保存和演化已进

246　行了广泛而深入的研究（Loucks et al., 2012; Katz and Arango, 2018; Liu et al., 2022）。有机孔隙的发育

247　取决于有机质类型和热成熟度，而其保存受控于有机质含量、页岩矿物组成和孔隙压力（Mastalerz et

248　al., 2013; Katz and Arango, 2018; 王濡岳等, 2020; Cao et al., 2021; Liu et al., 2022）。

249　3.1 有机孔隙发育

250　　　由于不同类型有机质的生烃潜力不同，有机孔隙发育程度也存在差异（Katz and Arango, 2018; 宋

251　董军等, 2019; Wu et al., 2020; Liu et al., 2022）。生油型有机质如藻类体和无定形体在热演化过程中转化

252　为油气和固体沥青或焦沥青（图 7）。随着油气的排出，固体沥青或焦沥青中产生孔隙（Bernard et al.,

253　2012; Cardott et al., 2015; Liu et al., 2017, 2019, 2022）。Bernard et al. (2012) 证明有机孔隙主要发育于焦

254　沥青中。Cardott et al. (2015) 在 Woodford 页岩中发现固体沥青中存在大量纳米孔隙。相互连通的沥青

255　网络可能形成一个在三级空间上相互连通的有机孔隙网络，不仅可以增强页岩的甲烷吸附能力和含气

256　量，而且可以提高孔隙度（Liu et al., 2022）。陆源有机质如镜质体和惰质体由于生烃潜力较低，其形

257　貌特征在热演化过程中未表现出明显变化，扫描电镜下检测不到有机孔隙（Liu et al., 2017），但镜质

258　体可能发育微孔（孔径< 2 nm），因为煤中的镜质体含有大量的微孔（Teng et al., 2017; Liu et al., 2018），

259　而这些微孔在扫描电镜下无法识别。惰质体虽然不发育次生孔隙，但可能含有原生孔隙，这些原生孔

260　隙来自植物的细胞结构，通常被自生矿物充填，孔径大小为几百纳米到几十微米（Liu et al., 2017,

261　2022）。动物碎屑如笔石和几丁虫的生烃能力与镜质体相当，其形貌特征在热演化过程中变化较小，在

262　高成熟度页岩中仍可被识别出。扫描电镜下，动物碎屑中有机孔隙基本不发育（Ardakani et al., 2018;

263　Yang et al., 2020），但多项研究在笔石中发现了有机孔隙（Luo et al., 2016; Ma et al., 2016; 邱振等, 2018;

264　Gong et al., 2020; 腾格尔等, 2021）。动物碎屑中有机孔隙的成因及其对页岩孔隙系统的贡献仍有待深入

265　研究。

266　　　次生有机孔隙一般认为是在有机质生烃和排烃过程中产生的，因此热成熟度对次生有机孔隙的发

267　育至关重要（Loucks et al., 2009, 2012; Schieber, 2010; Bernard et al., 2012; Curtis et al., 2012; Mastalerz et

268　al., 2013, 2018; Liu et al., 2017, 2022; Katz and Arango, 2018; 肖七林等, 2020）。一般认为有机孔隙开始发

269　育的热成熟度为 R_o 0.6%（Loucks et al. 2012），且有机孔隙的发育程度随成熟度的增加而升高。生气窗

270　内的有机孔隙比生油窗内更普遍，主要原因有两个：（1）生气窗内，气态烃的生成和排出更有利于生

271　成有机孔隙；（2）生油窗内沥青和油充填了新形成的有机孔隙，使有机孔隙不容易被识别（Liu et al.,

272　2019, 2022）。

273　3.2 有机孔隙保存

274　　　有机孔隙形成之后能否有效的保存是页岩气成藏的关键。页岩中有机质含量对有机孔隙的保存具

275　有控制作用（Katz and Arango, 2018; Liu et al., 2022）。有机质含量高的页岩硬度较低，在压实过程中有

机孔隙容易被破坏。Milliken et al. (2013) 对比了 Marcellus 页岩高 TOC 和低 TOC 样品，发现扫描电镜下，高 TOC 页岩的有机孔隙度较低，他们认为高 TOC 页岩经历了更强的机械压实作用，破坏了有机孔隙。页岩的矿物学组成同样影响有机孔隙的保存。富含生物成因硅和碳酸盐胶结物的页岩硬度较高，可以有效地保存有机孔隙（Fishman et al., 2012; Zhao et al., 2017; Dong and Harris, 2020; Knapp et al., 2020; Qiu et al., 2020），而粘土矿物含量较高的页岩由于硬度较低，有机孔隙在压实过程中容易被破坏（Fishman et al., 2012）。

外部因素如孔隙压力对有机孔隙的保存至关重要（王濡岳等, 2020; Cao et al., 2021）。孔隙超压对机械压实具有抑制作用，可以保持孔隙开放，保存有机孔隙。王濡岳等 (2020) 发现，随着压力系数的降低，有机孔隙由近圆形逐渐变为椭圆形、扁平或不规则状，孔径由数百纳米至微米减小至小于 50 nm。页岩气产量较高的井大多来自超压地层，如四川盆地焦石坝地区地层压力系数为 1.55（郭彤楼和张汉荣, 2014），页岩气产量较高，这与超压保存有机孔隙密切相关（王濡岳等, 2020; Cao et al., 2021）。页岩地层内超压的形成包括构造抬升、地层水升温、粘土矿物脱水、有机质生烃等因素（刘洪林等, 2016）。
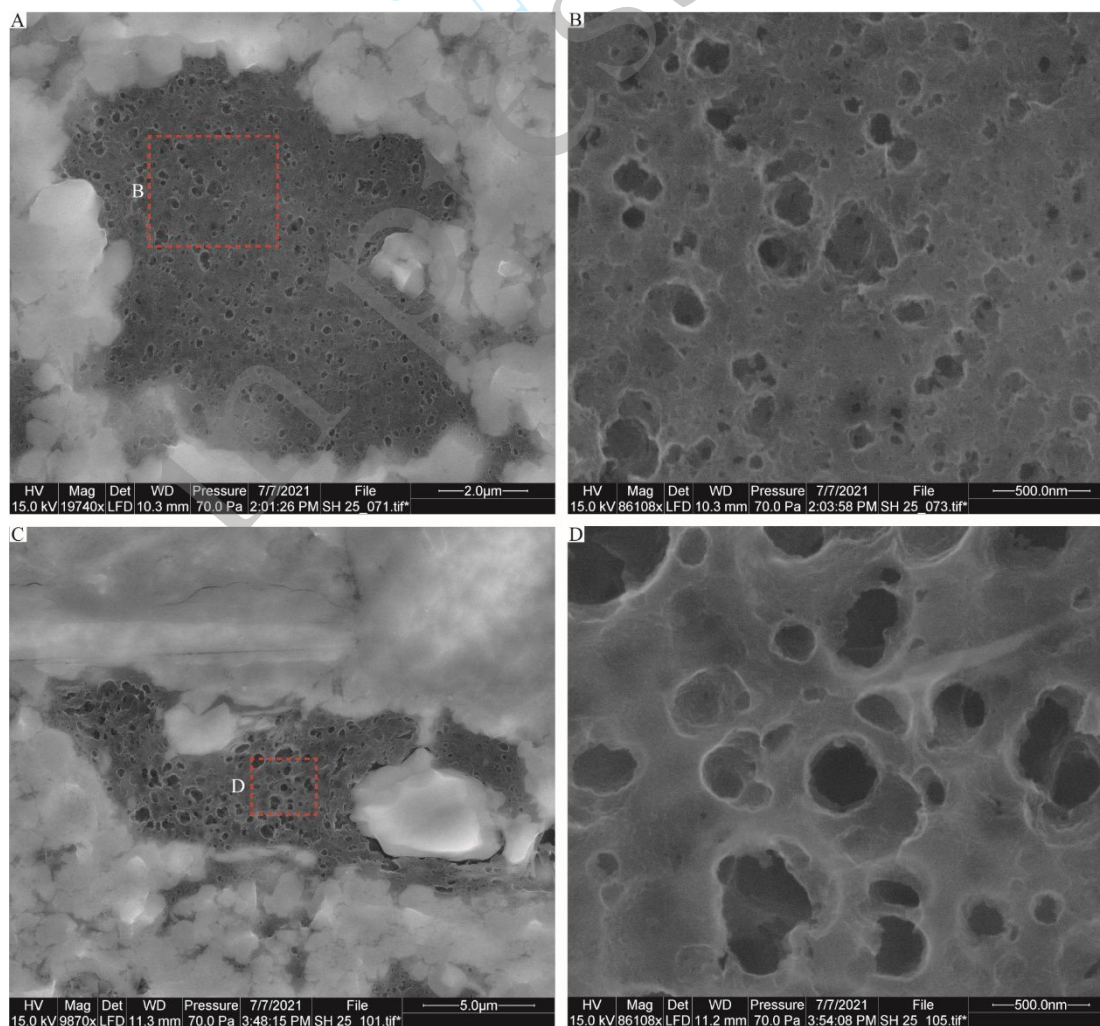
290 图 8 页岩中有机孔隙扫描电镜照片。四川盆地五峰组-龙马溪组页岩，等效镜质体反射率 EqR$_o$ 3.07%

291 Fig. 8 SEM images of organic matter-hosted pores in shales. Wufeng-Longmaxi Shale of the Sichuan Basin. Equivalent vitrinite

292 reflectance EqR$_o$ 3.07%

4 存在问题及今后研究方向

293

294 　　作为常规和非常规石油系统的生烃母质，泥页岩中分散有机质已经进行了广泛而深入的研究，但

295 仍存在诸多问题。首先，泥页岩中分散有机质类型的划分仍不清楚，是否将腐泥组单独划分为一个显

296 微组分组仍有待商榷，腐泥组主要包括藻类体和无定形体，而国际上一般把这两种显微组分划分到类

297 脂体中（Pickel et al., 2017; Mastalerz et al., 2018; Liu et al., 2022）。其次，沥青质体（bitiminite）与固体

298 沥青（solid bitumen）容易混淆。沥青质体为原生显微组分，是浮游植物经细菌降解而形成；而固体沥

299 青是次生显微组分，是生油型有机质生烃过程中的产物（Mastalerz et al., 2018）。然后，固体沥青和焦

300 沥青既可以来自生油型有机质热降解，又可以来自原油裂解，而生油型有机质包括多种显微组分，原

301 油由饱和烃、芳香烃、胶质和沥青质四个组分组成（卢双舫和张敏, 2008），如何利用固体沥青和焦沥

302 青的光学性质和化学结构特征区分不同物质来源和不同成因期次的沥青以及沥青成因对其物理化学性

303 质以及孔隙结构的控制作用仍有待深入研究。最后，有机孔隙是页岩储层中重要的孔隙类型，其形成、

304 保存和破坏已经进行了大量研究（Loucks et al., 2012; Milliken et al., 2013; Katz and Arango, 2018; Liu et

305 al., 2022）。有机孔隙的表征主要通过扫描电镜对 Ar 离子抛光的页岩表面进行观察和通过 N$_2$ 和 CO$_2$ 吸

306 附分析页岩中提纯的有机质。然而，扫描电镜成像无法检测孔径< 5 nm 的孔隙，而且扫描电镜研究区

307 域太过微观，无法定量表征有机孔隙。虽然 N$_2$ 和 CO$_2$ 吸附可以表征分离有机质的微观孔隙结构，但通

308 过酸溶解方法分离有机质往往无法完全去除黄铁矿等矿物，导致分离有机质并不纯净。酸化的氯化铬

309 （CrCl$_2$）（Acholla and Orr, 1993）处理或重液分离（French et al., 2020）可以有效地移除黄铁矿等矿物

310 （French et al., 2020）。建议对分离有机质表征之前进行 TOC 分析，验证分离有机质的纯度，如果分离

311 有机质含有较多矿物，建议对孔隙结构分析结果进行校正。值得注意的里，TOC 含量并不等于有机质

312 含量，因为有机质中还含有 N、S、O 等原子。而且酸溶解过程对有机质孔隙结构也有一定影响，例如

313 与矿物分离增加了有机质的外比表面积，但对有机质分子结构以及微观孔隙结构的影响尚不清楚，需

314 要进一步深入研究。

5 结语

315

316 　　泥页岩中的分散有机质可划分为 5 个显微组分组：镜质体、惰质体、类脂体、动物碎屑和次生有

317 机质，每个显微组分组又包含多个显微组分。页岩尤其是海相页岩中，镜质体和惰质体含量较少且粒

318 径较小，不适合划分显微组分。对于镜质体和惰质体含量较高的页岩，如煤系地层页岩，仍可按 ICCP

319 System 1994 镜质体和惰质体分类方案划分出不同的显微组分。页岩中常见的类脂体包括无定形体（又

320 称沥青质体）、藻类体和类脂碎屑体。

321 　　不同显微组分的成因不同，生烃潜力和有机孔隙发育程度也存在显著差异。生油型组分如藻类体

322 和无定形体在热演化过程中转化成油气和固体沥青或焦沥青，而镜质体、惰质体和动物碎屑在热演化

323 过程中形貌特征变化不明显。页岩中的有机孔隙包括原生孔隙和次生孔隙。原生孔隙主要来自植物的

324 胞腔，且多被成岩矿物充填，而次生孔隙在有机质生烃和排烃过程中产生，主要赋存在固体沥青或焦

325 沥青中。次生有机孔隙的发育受控于有机质类型和热成熟度，而其保存取决于热成熟度、有机质含量、

326 矿物组成以及孔隙压力。

致谢

参考文献

332 Acholla, F.V., Orr, W.L., 1993. Pyrite removal from kerogen without altering organic matter: the chromous chloride method.

333 *Energy & Fuels*, 7: 406−410. https://doi.org/10.1021/ef00039a012

334 Ardakani, O.H., Sanei, H., Ghanizadeh, A., et al., 2018. Do All Fractions of Organic Matter Contribute Equally in Shale

335 Porosity? A Case Study from Upper Ordovician Utica Shale, Southern Quebec, Canada. *Marine and Petroleum Geology*,

336 92: 794−808. https://doi.org/10.1016/j.marpetgeo.2017.12.009

337 Bertrand, R., Héroux, Y., 1987. Chitinozoan, Graptolite, and Scolecodont Reflectance as an Alternative to Vitrinite and

338 Pyrobitumen Reflectance in Ordovician and Silurian strata, Anticosti Island, Quebec, Canada. *AAPG Bulletin*, 71: 951−957.

339 https://doi.org/10.1306/948878F7-1704-11D7-8645000102C1865D

340 Bertrand, R., 1990. Correlations among the Reflectances of Vitrinite, Chitinozoans, Graptolites and Scolecodonts. *Organic

341 Geochemistry*, 15: 565−574. https://doi.org/10.1016/0146-6380(90)90102-6

342 Bernard, S., Horsfield, B., 2014. Thermal Maturation of Gas Shale Systems. *Annual Review of Earth and Planetary Sciences*, 42:

343 635−651. https://doi.org/10.1146/annurev-earth-060313-054850

344 Bernard, S., Horsfield, B., Schulz, H.M., et al., 2012. Geochemical Evolution of Organic-Rich Shales with Increasing Maturity:

345 A STXM and TEM Study of the Posidonia Shale (Lower Toarcian, northern Germany). *Marine and Petroleum Geology*, 31:

346 70−89. https://doi.org/10.1016/j.marpetgeo.2011.05.010

347 Bousige, C., Ghimbeu, C.M., Vix-Guterl, C., et al., 2016. Realistic Molecular Model of Kerogen's Nanostructure. *Nature

348 Materials*, 15: 576−582. https://doi.org/10.1038/nmat4541

349 Buchardt, B, Lewan, M.D., 1994. Reflectance of Vitrinite-Like Macerals as a Thermal Maturity Index for Cambrian–Ordovician

350 Alum Shale, Southern Scandinavia. *AAPG Bulletin*, 74: 394−406. https://doi.org/10.1306/0C9B230D-1710-11D7-

351 8645000102C1865D

352 Camp, W.K., 2016. Strategies for Identifying Organic Matter Types in SEM. AAPG Search and Discovery Article No. 70233.

353 Cao, Q., Jiang, K., Wen, Z.T., et al., 2021. Characteristics of Organic Matter Pores and the Relationship with Current Pressure

354 System of Lower Silurian Longmaxi Shales in Dingshan Field, Southern Sichuan, China. Geofluids, 2021: 9967479.

355   https://doi.org/10.1155/2021/9967479

356   Cardott, B.J., Landis, C.R., Curtis, M.E., 2015. Post-Oil Solid Bitumen Network in the Woodford Shale, USA—A Potential
357   Primary   Migration   Pathway.   *International   Journal   of   Coal   Geology*,   139:   106–113.
358   https://doi.org/10.1016/j.coal.2014.08.012

359   Chen, G.H., Lu, S.F., Liu, K.Y., et al., 2020. Occurrence State and Micro Mechanisms of Shale Gas on Pore Walls. *Earth
360   Science*, 45(5): 1782–1790 (in Chinese with English abstract).

361   Curtis, M.E., Cardott, B.J., Sondergeld, C.H., et al., 2012. Development of Organic Porosity in the Woodford Shale with
362   Increasing Thermal Maturity. *International Journal of Coal Geology*, 103: 26–31. https://doi.org/10.1016/j.coal.2012.08.004

363   Dai, S.F., Tang, Y.G., Jiang, Y.F., et al., 2021a. An in-depth Interpretation of Definition and Classification of Macerals in Coal
364   (ICCP system 1994) for Chinese Researchers, I: Vitrinite. *Journal of China Coal Society*, 46(6): 1821–1832 (in Chinese
365   with English abstract).

366   Dai, S.F., Wang, S.Q., Tang, Y.G., et al., 2021b. An in-depth Interpretation of Definition and Classification of Macerals in Coal
367   (ICCP system 1994) for Chinese Researchers, II: Inertinite. *Journal of China Coal Society*, 46(7): 2212–2226 (in Chinese
368   with English abstract).

369   Dai, S.F., Zhao, L., Tang, Y.G., et al., 2021c. An in-depth Interpretation of Definition and Classification of Macerals in Coal
370   (ICCP system 1994) for Chinese Researchers, III: Liptinite. *Journal of China Coal Society*, 46(9): 2965–2983 (in Chinese
371   with English abstract).

372   Dong, T., Harris, N.B., 2020. The Effect of Thermal Maturity on Porosity Development in the Upper Devonian–Lower
373   Mississippian Woodford Shale, Permian Basin, US: Insights into the Role of Silica Nanospheres and Microcrystalline
374   Quartz   on   Porosity   Preservation.   *International   Journal   of   Coal   Geology*,   217:   103346.
375   https://doi.org/10.1016/j.coal.2019.103346

376   Durand, B., 1980. Sedimentary Organic Matter and Kerogen: Definition and Quantitative Importance of Kerogen. In: Kerogen:
377   Insoluble Organic Matter from Sedimentary Rocks. Editions Technip, Paris, 13–34.

378   Feng, G.X., Chen, S.J., 1988. Relationship between the Reflectance of Bitumen and Vitrinite in Rock. *Natural Gas Industry*,
379   8(3): 20–25 (in Chinese with English abstract).

380   Fishman, N.S., Hackley, P.C., Lowers, H.A., et al., 2012. The Nature of Porosity in Organic-Rich Mudstones of the Upper
381   Jurassic Kimmeridge Clay Formation, North Sea, Offshore United Kingdom. *International Journal of Coal Geology*, 103:
382   32−50. https://doi.org/10.1016/j.coal.2012.07.012

383   Flores, D., Suárez-Ruiz, I., 2017. Organic Petrology in the study of Dispersed Organic Matter. In: The Role of Organic Petrology
384   in the Exploration of Conventional and Unconventional Hydrocarbon Systems. Bentham Science Publishers, Sharjah,
385   34−76.

386   French, K.L., Birdwell, J.E., Lewan, M.D., 2020. Trends in Thermal Maturity Indicators for the Organic Sulfur-rich Eagle Ford
387   Shale. *Marine and Petroleum Geology*, 118: 104459. https://doi.org/10.1016/j.marpetgeo.2020.104459

388   Gong, J.M., Qiu, Z., Zou, C.N., et al., 2020. An Integrated Assessment System for Shale Gas Resources Associated with
389   Graptolites and Its Application. *Applied Energy*, 262: 114524. https://doi.org/10.1016/j.apenergy.2020.114524

390   Goodarzi, F., Norford, B.S., 1989. Variation of Graptolite Reflectance with Depth of Burial. *International Journal of Coal*

391   *Geology*, 11: 127–141. https://doi.org/10.1016/0166-5162(89)90002-5

392   Guo, T.L., Zhang, H.R., 2014. Formation and Enrichment Mode of Jiaoshiba Shale Gas Field, Sichuan Basin. *Petroleum*
393   *Exploration and Development*, 41(1): 28–36 (in Chinese with English abstract).

394   Hackley, P.C., Cardott, B.J., 2016. Application of Organic Petrography in North American Shale Petroleum Systems: A Review.
395   *International Journal of Coal Geology*, 163: 8−51. https://doi.org/10.1016/j.coal.2016.06.010

396   Hackley, P.C., Walters, C.C., Kelemen, S.R., 2017. Organic Petrology and Micro-spectroscopy of Tasmanites Microfossils:
397   Applications to Kerogen Transformations in the Early Oil Window. Organic Geochemistry, 114: 23−44.
398   https://doi.org/10.1016/j.orggeochem.2017.09.002

399   Han, D.X., 1996. Coal Petrology of China. China University of Mining & Technology Press, Beijing (in Chinese).

400   Hao, F., Zou, H.Y., Lu, Y.C., 2013. Mechanisms of Shale Gas Storage: Implications for Shale Gas Exploration in China. *AAPG*
401   *Bulletin*, 97: 1325−1346. https://doi.org/10.1306/02141312091

402   ICCP, 1998. The New Vitrinite Classification (ICCP System 1994). *Fuel*, 77: 349−358. https://doi.org/10.1016/S0016-
403   2361(98)80024-0

404   ICCP, 2001. The New Inertinite Classification (ICCP System 1994). *Fuel*, 80: 459−471. https://doi.org/10.1016/S0016-
405   2361(00)00102-2

406   Jacob, H., 1989. Classification, Structure, Genesis and Practical Importance of Natural Solid Oil Bitumen ("Migrabitumen").
407   *International Journal of Coal Geology*, 11: 65−79. https://doi.org/10.1016/0166-5162(89)90113-4

408   Jarvie, D.M., Hill, R.J., Ruble, T.E., et al., 2007. Unconventional Shale-gas Systems: The Mississippian Barnett Shale of North-
409   central Texas as One Model for Thermogenic Shale-gas Assessment. *AAPG Bulletin*, 91: 475−499.
410   https://doi.org/10.1306/12190606068

411   Jarvie, D.M., 2012a. Shale Resource Systems for Oil and Gas: Part 1—Shale-Gas Resource Systems. In: Shale Reservoirs—
412   Giant Resources for the 21st Century. AAPG Memoir 97, AAPG, Tulsa, 69–87. DOI:10.1306/13321446M973489

413   Jarvie, D.M., 2012b. Shale Resource Systems for Oil and Gas: Part 2—Shale-Oil Resource Systems. In: Shale Reservoirs—
414   Giant Resources for the 21st Century. AAPG Memoir 97, AAPG, Tulsa, 89–119. DOI:10.1306/13321447M973489

415   Katz, B.J., Arango, I., 2018. Organic Porosity: A Geochemist's View of the Current State of Understanding. *Organic*
416   *Geochemistry*, 123: 1–16. https://doi.org/10.1016/j.orggeochem.2018.05.015

417   Knapp, L.J., Ardakani, O.H., Uchida, S., et al., 2020. The Influence of Rigid Matrix Minerals on Organic Porosity and Pore Size
418   in Shale Reservoirs: Upper Devonian Duvernay Formation, Alberta, Canada. *International Journal of Coal Geology*, 227:
419   103525. https://doi.org/10.1016/j.coal.2020.103525

420   Kus, J., Araujo, C.V., Borrego, A.G., et al., 2017. Identification of Alginite and Bituminite in Rocks Other than Coal. 2006, 2009,
421   and 2011 Round Robin Exercises of the ICCP Identification of Dispersed Organic Matter Working Group. *International*
422   *Journal of Coal Geology*, 178: 26−38. https://doi.org/10.1016/j.coal.2017.04.013

423   Landis, C.R., Castaño, J.R., 1995. Maturation and Bulk Chemical Properties of a Suite of Solid Hydrocarbons. *Organic*
424   *Geochemistry*, 22: 137−149. https://doi.org/10.1016/0146-6380(95)90013-6

425   Liu, B., Schieber, J., Mastalerz, M., 2017. Combined SEM and Reflected Light Petrography of Organic Matter in the New

426   Albany Shale (Devonian-Mississippian) in the Illinois Basin: A Perspective on Organic Pore Development with Thermal
427   Maturation. *International Journal of Coal Geology*, 184: 57−72. https://doi.org/10.1016/j.coal.2017.11.002

428   Liu, B., Schieber, J., Mastalerz, M., 2019. Petrographic and Micro-FTIR Study of Organic Matter in the Upper Devonian New
429   Albany Shale during Thermal Maturation: Implications for Kerogen Transformation. In: Mudstone Diagenesis: Research
430   Perspectives for Shale Hydrocarbon Reservoirs, Seals, and Source Rocks. AAPG Memoir 120, AAPG, Tulsa, 165–188.
431   DOI: 10.1306/13672216M1213380

432   Liu, B., Mastalerz, M., Schieber, J., et al., 2020a. Association of Uranium with Macerals in Marine Black Shales: Insights from
433   the Upper Devonian New Albany Shale, Illinois Basin. *International Journal of Coal Geology*, 217: 103351.
434   https://doi.org/10.1016/j.coal.2019.103351

435   Liu, B., Teng, J., Mastalerz, M., et al., 2020b. Assessing the Thermal Maturity of Black Shales using Vitrinite Reflectance:
436   Insights from Devonian Black Shales in the Eastern United States. *International Journal of Coal Geology*, 220: 103426.
437   https://doi.org/10.1016/j.coal.2020.103426

438   Liu, B., Teng, J., Mastalerz, M., et al., 2021. Compositional Control on Shale Pore Structure Characteristics across a Maturation
439   Gradient: Insights from the Devonian New Albany Shale and Marcellus Shale in the Eastern United States. *Energy & Fuels*,
440   2021, 35: 7913−7929. https://doi.org/10.1021/acs.energyfuels.1c00526

441   Liu, B., Mastalerz, M., Schieber, J., 2022. SEM Petrography of Dispersed Organic Matter in Black Shales: A Review. *Earth-*
442   *Science Reviews*, 224: 103874. https://doi.org/10.1016/j.earscirev.2021.103874

443   Liu, D.M., Jin, K.L., Ai, T.J., 1995. A Petrographic Classification and Organic Petrological Characteristics of Macerals of the
444   Marine Hydrocarbon Source Rocks in the Tarim Basin. *Acta Sedimentologica Sinica*, 13: 124–133 (in Chinese with English
445   abstract).

446   Liu, H.L., Wang, H.Y., Fang, C.H., et al., 2020. The Formation Mechanism of Over-pressure Reservoir and Target Screening
447   Index of the Marine Shale in the South China. *Earth Science Frontiers*, 23(2): 48–54 (in Chinese with English abstract).

448   Liu, Y., Zhu, Y.M., Liu, S.M., et al., 2018. Molecular Structure Controls on Micropore Evolution in Coal Vitrinite during
449   Coalification. *International Journal of Coal Geology*, 199: 19–30. https://doi.org/10.1016/j.coal.2018.09.012

450   Loucks, R.G., Reed, R.M., Ruppel, S.C., et al., 2009. Morphology, Genesis, and Distribution of Nanometer-Scale Pores in
451   Siliceous Mudstones of the Mississippian Barnett Shale. *Journal of Sedimentary Research*, 79: 848−861.
452   https://doi.org/10.2110/jsr.2009.092

453   Loucks, R.G., Reed, R.M., Ruppel, S.C., et al., 2012. Spectrum of Pore Types and Networks in Mudrocks and a Descriptive
454   Classification for Matrix-Related Mudrock Pores. *AAPG Bulletin*, 96: 1071−1098. https://doi.org/10.1306/08171111061

455   Lu, S.F., Zhang, M., 2008. Oil and Gas Geochemistry. Petroleum Industry Press, Beijing (in Chinese).

456   Luo, Q.Y., Zhong, N.N., Dai, N., et al., 2016. Graptolite-Derived Organic Matter in the Wufeng–Longmaxi Formations (Upper
457   Ordovician–Lower Silurian) of Southeastern Chongqing, China: Implications for Gas Shale Evaluation. *International*
458   *Journal of Coal Geology*, 153: 87−98. https://doi.org/10.1016/j.coal.2015.11.014

459   Luo, Q.Y., Hao, J.Y., Skovsted, C.B., et al., 2017. The Organic Petrology of Graptolites and Maturity Assessment of the
460   Wufeng–Longmaxi Formations from Chongqing, China: Insights from Reflectance Cross-Plot Analysis. *International*
461   *Journal of Coal Geology*, 183: 161−173. https://doi.org/10.1016/j.coal.2017.09.006

462 Luo, Q.Y., Fariborz, G., Zhong, N.N., et al., 2020. Graptolites as Fossil Geo-Thermometers and Source Material of
463   Hydrocarbons: An Overview of Four Decades of Progress. *Earth-Science Reviews*, 200: 103000.
464   https://doi.org/10.1016/j.earscirev.2019.103000

465 Ma, Y., Zhong, N.N., Cheng, L.J., et al., 2016. Pore Structure of the Graptolite-derived OM in the Longmaxi Shale, Southeastern
466   Upper Yangtze Region, China. Marine and Petroleum Geology, 72: 1−11. https://doi.org/10.1016/j.marpetgeo.2016.01.009

467 Mastalerz, M., Schimmelmann, A., Drobniak, A., et al., 2013. Porosity of Devonian and Mississippian New Albany Shale across
468   a Maturation Gradient: Insights from Organic Petrology, Gas Adsorption, and Mercury Intrusion. *AAPG Bulletin*, 97:
469   1621−1643. https://doi.org/10.1306/04011312194

470 Mastalerz, M., Drobniak, A., Stankiewicz, A.B., 2018. Origin, Properties, and Implications of Solid Bitumen in Source-Rock
471   Reservoirs: A Review. *International Journal of Coal Geology*, 195: 14−36. https://doi.org/10.1016/j.coal.2018.05.013

472 Milliken, K.L., Rudnicki, M., Awwiller, D.N., et al., 2013. Organic Matter–Hosted Pore System, Marcellus Formation
473   (Devonian), Pennsylvania. *AAPG Bulletin*, 97: 177−200. https://doi.org/10.1306/07231212048

474 Mukhopadhyay, P.K., Dow, W.G., 1994. Vitrinite Reflectance as A Maturity Parameter: Applications and Limitations. ACS
475   Symposium Series 570, American Chemical Society, Washington, DC.

476 Passey, Q.R., Bohacs, K.M., Esch, W.L., et al., 2010. From oil-prone source rock to gas-producing shale reservoir-geologic and
477   petrophysical characterization of unconventional shale-gas reservoirs. Chinese Petroleum Society/Society of Petroleum
478   Engineers International Oil and Gas Conference and Exhibition, Beijing, China, SPE 131350.

479 Peters, K.E., Cassa, M.R., 1994. Applied Source Rock Geochemistry. In: The Petroleum System—From Source to Trap. AAPG
480   Memoir 60, AAPG, Tulsa, 93−120.

481 Petersen, H.I., Schovsbo, N.H., Nielsen, A.T., 2013. Reflectance Measurements of Zooclasts and Solid Bitumen in Lower
482   Paleozoic Shales, Southern Scandinavia: Correlation to Vitrinite Reflectance. *International Journal of Coal Geology*, 114:
483   1−18. https://doi.org/10.1016/j.coal.2013.03.013

484 Pickel, W., Kus, J., Flores, D., et al., 2017. Classification of Liptinite–ICCP System 1994. *International Journal of Coal
485   Geology*, 169: 40−61. https://doi.org/10.1016/j.coal.2016.11.004

486 Potter, J., Stasiuk, L.D., Cameron, A.R., 1998. A Petrographic Atlas of Canadian Coal Macerals and Dispersed Organic Matter.
487   Calgary. Canadian Society for Coal Science and Organic Petrology–Geological Survey of Canada (Calgary)-Canmet Energy
488   Technology Centre, Calgary.

489 Qiu, Z., Zou, C.N., Li, X.Z., et al., 2018. Discussion on the Contribution of Graptolite to Organic Enrichment and Gas Shale
490   Reservoir: A Case Study of the Wufeng–Longmaxi Shales in South China. *Journal of Natural Gas Geoscience*, 29(5): 606–
491   615 (in Chinese with English abstract).

492 Qiu, Z., Liu, B., Dong, D., et al., 2020. Silica Diagenesis in the Lower Paleozoic Wufeng and Longmaxi Formations in the
493   Sichuan Basin, South China: Implications for Reservoir Properties and Paleoproductivity. *Marine and Petroleum Geology*,
494   121: 104594. https://doi.org/10.1016/j.marpetgeo.2020.104594

495 Qiu, Z., Zou, C.N., Wang, H.Y., et al., 2020. Discussion on the Characteristics and Controlling Factors of Differential
496   Enrichment of Shale Gas in the Wufeng-Longmaxi Rormations in south China. *Journal of Natural Gas Geoscience*, 31(2):
497   163–175 (in Chinese with English abstract).

498 Ross, D.J.K., Bustin, R.M., 2009. The Importance of Shale Composition and Pore Structure upon Gas Storage Potential of Shale
499   Gas Reservoirs. *Marine and Petroleum Geology*, 26: 916−927. https://doi.org/10.1016/j.marpetgeo.2008.06.004

500 Ryder, R.T., Hackley, P.C., Alimi, H., et al., 2013. Evaluation of Thermal Maturity in the Low Maturity Devonian Shales of the
501   Northern Appalachian Basin. AAPG Eastern Section Meeting, Kalamazoo, Michigan, USA, 2013, AAPG Search and
502   Discovery Article No. 10477.

503 Sanei, H., 2020. Genesis of Solid Bitumen. *Scientific Reports*, 10: 1−10. https://doi.org/10.1038/s41598-020-72692-2

504 Schieber, J., 2010. Common Themes in the Formation and Preservation of Intrinsic Porosity in Shales and Mudstones-Illustrated
505   with Examples across the Phanerozoic. SPE Unconventional Gas Conference, Pittsburgh, Pennsylvania, USA. 2010, SPE
506   132370.

507 Schieber, J., 2013. SEM Observations on Ion-Milled Samples of Devonian Black Shales from Indiana and New York: The
508   Petrographic Context of Multiple Pore Types. In: Electron Microscopy of Shale Hydrocarbon Reservoirs. AAPG Memoir
509   102, AAPG, Tulsa, 153−171.

510 Schmidt, J.S., Menezes, T.R., Souza, I.V.A.F., et al., 2019. Comments on Empirical Conversion of Solid Bitumen Reflectance for
511   Thermal Maturity Evaluation. *International Journal of Coal Geology*, 201: 44–50.
512   https://doi.org/10.1016/j.coal.2018.11.012

513 Schoenherr, J., Littke, R., Urai, J.L., et al., 2007. Polyphase Thermal Evolution in the Infra-Cambrian Ara Group (South Oman
514   Salt Basin) as Deduced by Maturity of Solid Reservoir Bitumen. *Organic Geochemistry*, 38: 1293−1318.
515   https://doi.org/10.1016/j.orggeochem.2007.03.010

516 Senftle, J.T., Brown, J.H., Larter, S.R., 1987. Refinement of Organic Petrographic Methods for Kerogen Characterization.
517   *International Journal of Coal Geology*, 7: 105−117. https://doi.org/10.1016/0166-5162(87)90015-2

518 Song, D.J., Tuo, J.C., Wang, Y.T., et al., 2019. Research Advances on Characteristics of Nanopore Structure of Organic-Rich
519   Shales. *Acta Sedimentologica Sinica*, 2019, 37(6): 1309–1324 (in Chinese with English abstract).

520 Stasiuk, L.D., 1997. The Origin of Pyrobitumens in Upper Devonian Leduc Formation Gas Reservoirs, Alberta, Canada: An
521   Optical and EDS Study of Oil to Gas Transformation. *Marine and Petroleum Geology*, 14: 915−929.
522   https://doi.org/10.1016/S0264-8172(97)00031-7

523 Stasiuk, L.D., Burgess, J., Thompson-Rizer, C., et al., 2002. Status Report on TSOP-ICCP Dispersed Organic Matter
524   Classification Working Group. The Society for Organic Petrology Newsletter, 19(3): 14.

525 Taylor, G.H., Teichmüller, M., Davis, A. et al., 1998. Organic Petrology. Gebrüder Borntraeger, Berlin-Stuttgart.

526 Teichmüller, M., 1986. Organic Petrology of Source Rocks, History and State of the Art. *Organic Geochemistry*, 10: 581–599.
527   https://doi.org/10.1016/0146-6380(86)90055-0

528 Tenger, B., Lu, L.L., Yu, L.J., et al., 2021. Formation, Preservation and Connectivity Control of Organic Pores in Shale.
529   *Petroleum Exploration and Development*, 48(4): 687–699 (in Chinese with English abstract).

530 Teng, J., Mastalerz, M., Hampton, L., 2017. Maceral Controls on Porosity Characteristics of Lithotypes of Pennsylvanian High
531   Volatile Bituminous Coal: Example from the Illinois Basin. *International Journal of Coal Geology*, 2017, 172: 80−94.
532   https://doi.org/10.1016/j.coal.2017.02.001

533 Teng, J., Mastalerz, M., Liu, B., 2021. Petrographic and Chemical Structure Characteristics of Amorphous Organic Matter in

534   Marine Black Shales: Insights from Pennsylvanian and Devonian Black Shales in the Illinois Basin. *International Journal of*

535   *Coal Geology*, 235: 103676. https://doi.org/10.1016/j.coal.2021.103676

536   Tissot B.P., Welte, D.H., 1984. Petroleum Formation and Occurrence, 2nd ed. Springer-Verlag, Berlin.

537   Thompson, C.L., Dembicki Jr, H., 1986. Optical Characteristics of Amorphous Kerogens and the Hydrocarbon-Generating

538   Potential of Source Rocks. *International Journal of Coal Geology*, 6: 229–249. https://doi.org/10.1016/0166-

539   5162(86)90003-0

540   Tu, J.Q., Wang, S.Z., Fei, X.D., 1998. Discussion on Certain Problems to the Division of Organic Matter Types in Kerogen.

541   *Experimental Petroleum Geology*, 20(2): 187–191 (in Chinese with English abstract).

542   Tu, J.Q., Chen, J.P., Zhang, D.J., et al., 2012. A Petrographic Classification of Macerals in Lacustrine Carbonate Source Rocks

543   and Their Organic Petrological Characteristics: A Case Study on Jiuxi Basin, NW China. *Acta Petrologica Sinica*, 28(3):

544   917–926 (in Chinese with English abstract).

545   Vigran, J.O., Mørk, A., Forsberg, A.W., et al., 2008. Tasmanites Algae—Contributors to the Middle Triassic Hydrocarbon

546   Source Rocks of Svalbard and the Barents Shelf. *Polar Research*, 27: 360−371. https://doi.org/10.1111/j.1751-

547   8369.2008.00084.x

548   Wang, B.Z., Wang, C.S., Wang, X.F., et al., 2019. Characteristics of Aromatic Compounds in High-over Matured Marine Shale

549   and Its Significance to Shale Gas. *Earth Science*, 44(11): 3705–3716 (in Chinese with English abstract).

550   Wang, F.Y., Fu, J.M., Liu, D.H., 1993. Source Rock Characteristics of Coal and Terrestrial Organic Matter and Maceral

551   Classification. *Chinese Science Bulletin,* 38(23): 2164–2168 (in Chinese with English abstract).

552   Wang, R.Y., Nie, H.K., Hu, Z.Q., et al., 2020. Controlling Effect of Pressure Evolution on Shale Gas Reservoirs: A Case Study

553   of the Wufeng–Longmaxi Formation in the Sichuan Basin. *Natural Gas Industry*, 40(10): 1–11 (in Chinese with English

554   abstract).

555   Wang, Y., Qiu, N.S., Yang, Y.F., et al., 2019. Thermal Maturity of Wufeng-Longmaxi Shale in Sichuan Basin. *Earth Science*,

556   44(3): 953–971 (in Chinese with English abstract).

557   Wang, Y., Qiu, N.S., Ma, Z.L., et al., 2020. Evaluation of Equivalent Relationship Between Vitrinite Reflectance and Solid

558   Bitumen Reflectance. *Journal of China University of Mining & Technology*, 49(3): 563−575 (in Chinese with English

559   abstract).

560   Wang, Y.M., Dong, D.Z., Cheng, X.Z., et al., 2014. Electric Property Evidences of the Carbonification of Organic Matters in

561   Marine Shales and Its Geologic Significance: A Case of the Lower Cambrian Qiongzhusi Shale in Southern Sichuan Basin.

562   *Natural Gas Industry*, 34(8): 1−7 (in Chinese with English abstract).

563   Wu, Z.R., He, S., Han, Y.J., et al., 2020. Effect of Organic Matter Type and Maturity on Organic Matter Pore Formation of

564   Transitional Facies Shales: A Case Study on Upper Permian Longtan and Dalong Shales in Middle Yangtze Region, China.

565   *Journal of Earth Science*, 31: 368–384.

566   Xiao, Q.L., Liu, A., Li, C.X., et al., 2020. Formation and Evolution of Nanopores in Highly Matured Shales at Over-mature

567   Stage: Insights from the Hydrous Pyrolysis Experiments on Cambrain Shuijintuo Shale from the Middle Yangtze Region.

568   *Earth Science*, 45(6): 2160–2171 (in Chinese with English abstract).

569   Xiao, X.M., Jin, K.L., 1990. A Petrographic Classification of Macerals in Terrestrial Hydrocarbon Source Rocks in China and

570   Their Organic Petrological Characteristics. *Acta Sedimentologica Sinica*, 8(3): 22–34 (in Chinese with English abstract).

571 Xiao, X.M., Jin, K.L., 1991. Hydrocarbon Generation Characteristics of Macerals. *Chinese Science Bulletin*, (3): 208–211 (in
572   Chinese with English abstract).

573 Xu, X.M., Sun, W.L., Wang, S.Q., et al., 2019. Maturity Evaluation of Marine Shale in the Lower Paleozoic in South China.
574   *Earth Science*, 44(11): 3717–3724 (in Chinese with English abstract).

575 Yang, C., Xiong, Y., Zhang, J., 2020. A Comprehensive Re-understanding of the OM-hosted Nanopores in the Marine Wufeng–
576   Longmaxi Shale Formation in South China by Organic Petrology, Gas Adsorption, and X-ray Diffraction Studies.
577   I*nternational Journal of Coal Geology*, 218: 103362. https://doi.org/10.1016/j.coal.2019.103362

578 Yang, Y.F., 2016. Application of Bitumen and Graptolite Reflectance in the Silurian Longmaxi Shale, Southeastern Sichuan
579   Basin. *Petroleum Geology & Experiment*, 38(4): 466–472 (in Chinese with English abstract).

580 Zhao, J.H., Jin, Z.K., Jin, Z.J., et al., 2017. Origin of Authigenic Quartz in Organic-Rich Shales of the Wufeng and Longmaxi
581   Formations in the Sichuan Basin, South China: Implications for Pore Evolution. *Journal of Natural Gas Science and*
582   *Engineering*, 38: 21−38. https://doi.org/10.1016/j.jngse.2016.11.037

583 Zhao, W.Z., Jia, A.L., Wei, Y.S., et al., 2020. Progress in Shale Gas Exploration in China and Prospects for Future Development.
584   China *Petroleum Exploration*, 25(1): 31–44 (in Chinese with English abstract).

585 Zou, C.N., Pan, S.Q., Jing, Z.H., et al., 2020. Shale Oil and Gas Revolution and Its Impact. *Acta Petrolei Sinica*, 41(1): 1−12 (in
586   Chinese with English abstract).

587 Zou, C.N., Qiu, Z., 2021. New advances in unconventional petroleum sedimentology in China. *Acta Sedimentologica*, 39(1): 1−9
588   (in Chinese with English abstract).

589

590 **附中文参考文献**

591 陈国辉, 卢双舫, 刘可禹, 等, 2020. 页岩气在孔隙表面的赋存状态及其微观作用机理. 地球科学, 45(5): 1782–1790.

592 代世峰, 唐跃刚, 姜尧发, 等, 2021a. 煤的显微组分定义与分类(ICCP system 1994)解析I: 镜质体. 煤炭学报, 46(6): 1821–
593   1832.

594 代世峰, 王绍清, 唐跃刚, 等, 2021b. 煤的显微组分定义与分类(ICCP system 1994)解析II: 惰质体. 煤炭学报, 46(7): 2212–
595   2226.

596 代世峰, 赵蕾, 唐跃刚, 等, 2021c. 煤的显微组分定义与分类(ICCP system 1994)解析III: 类脂体. 煤炭学报, 46(9): 2965–
597   2983.

598 丰国秀, 陈盛吉, 1988. 岩石中沥青反射率与镜质体反射率之间的关系. 天然气工业, 8(3): 20–25.

599 郭彤楼, 张汉荣, 2014. 四川盆地焦石坝页岩气田形成与富集高产模式. 石油勘探与开发, 41(1): 28–36.

600 韩德馨, 1996. 中国煤岩学. 北京: 中国矿业大学出版社.

601 刘大锰, 金奎励, 艾天杰, 1995. 塔里木盆地海相烃源岩显微组分的分类及其岩石学特征. 沉积学报, 13: 124–133.

602 刘洪林, 王红岩, 方朝合, 等, 2016. 中国南方海相页岩气超压机制及选区指标研究. 地学前缘, 23(2): 48–54.

603 卢双舫, 张敏, 2008. 油气地球化学. 北京: 石油工业出版社.

604 邱振, 邹才能, 李熙喆, 等, 2018,. 论笔石对页岩气源储的贡献——以华南地区五峰组-龙马溪组笔石页岩为例. 天然气地球

605 　　科学, 29(5): 606–615.

606 邱振, 邹才能, 王红岩, 等, 2020. 中国南方五峰组—龙马溪组页岩气差异富集特征与控制因素. 天然气地球科学, 31(2):
607 　　163–175.

608 宋董军, 妥进才, 王晔桐, 等, 2019. 富有机质泥页岩纳米级孔隙结构特征研究进展. 沉积学报, 37(6): 1309–1324.

609 腾格尔, 卢龙飞, 俞凌杰, 等, 2021. 页岩有机质孔隙形成、保持及其连通性的控制作用. 石油勘探与开发, 48(4): 687–699.

610 涂建琪, 王淑芝, 费轩冬, 1998. 干酪根有机质类型划分的若干问题的探讨. 石油实验地质, 20(2): 187–191.

611 涂建琪, 陈建平, 张大江, 等, 2012. 湖相碳酸盐岩烃源岩有机显微组分分类及其岩石学特征——以酒西盆地为例. 岩石学
612 　　报, 28(3): 917–926.

613 王保忠, 王传尚, 汪啸风, 等, 2019. 海相高过成熟页岩芳烃特征及页岩气意义. 地球科学, 44(11): 3705–3716.

614 王飞宇, 傅家谟, 刘德汉, 1993. 煤和陆源有机质烃源岩特点和有机组分分类术. 科学通报, 38(23): 2164–2168.

615 王濡岳, 聂海宽, 胡宗全, 2020. 压力演化对页岩气储层的控制作用—以四川盆地五峰组—龙马溪组为例. 天然气工业,
616 　　40(10): 1–11.

617 王晔, 邱楠生, 仰云峰, 等, 2019. 四川盆地五峰-龙马溪组页岩成熟度研究. 地球科学, 44(3): 953–971.

618 王晔, 邱楠生, 马中良, 等, 2020. 固体沥青反射率与镜质体反射率的等效关系评价. 中国矿业大学学报, 49(3): 563−575.

619 王玉满, 董大忠, 程相志, 等, 2014. 海相页岩有机质碳化的电性证据及其地质意义—以四川盆地南部地区下寒武统筇竹寺
620 　　组页岩为例. 天然气工业, 34(8): 1−7.

621 肖七林, 刘安, 李楚雄, 等, 2020. 高演化页岩纳米孔隙在过熟阶段的形成演化特征及主控因素: 中扬子地区寒武系水井沱
622 　　组页岩含水热模拟实验. 地球科学, 45(6): 2160–2171.

623 肖贤明, 金奎励, 1990. 中国陆相源岩显微组分的分类及其岩石学特征. 沉积学报, 8(3): 22–34.

624 肖贤明, 金奎励, 1991. 显微组分的成烃作用模式. 科学通报, (3): 208–211.

625 徐学敏, 孙玮琳, 汪双清, 等, 2019. 南方下古生界海相页岩有机质成熟度评价. 地球科学, 44(11): 3717–3724.

626 仰云峰, 2016. 川东南志留系龙马溪组页岩沥青反射率和笔石反射率的应用. 石油实验地质, 38(4): 466–472.

627 赵文智, 贾爱林, 位云生, 等, 2020. 中国页岩气勘探开发进展及发展展望. 中国石油勘探, 2020, 25(1): 31–44.

628 邹才能, 潘松圻, 荆振华, 等, 2020. 页岩油气革命及影响. 石油学报, 41(1): 1–12.

629 邹才能, 邱振, 2021. 中国非常规油气沉积学新进展. 沉积学报, 39(1): 1–9.

630